

The influence of the load level during cyclic torsion on the fatigue life and fracture surface of tin-zinc-lead bronze RG7

Joanna Małecka^{1*} , Krzysztof Żak¹ , Tadeusz Łagoda¹ 

¹ Opole University of Technology ul. Prószkowska 76 45-758 Opole, Poland

* Corresponding author's e-mail: j.malecka@po.edu.pl

ABSTRACT

The study analysed samples made of tin-zinc-lead bronze RG7 after fatigue tests under cyclic torsion conditions. The behaviour of the material used in both mechanical and building structures was analysed. Samples made for various load levels were subjected to this analysis. Fatigue cracks during cyclic torsion of samples made of RG7 bronze were analysed for nine load levels. Fatigue crack surfaces were analysed, with particular emphasis on the crack direction. For lower loads, the macroscopic fatigue crack surface is inclined at an average angle of 40°. The angle of the inclined plane of the cyclic torsion crack tends to decrease with increasing stress amplitude. The less load the tested samples carry, the more uniform the appearance of the crack surface. In the case of samples tested at lower stresses, a crack zone was observed in the lower part of the crack, which was damaged in the final phase of the test. This part of the crack was characterised by a rougher surface, where the tearing of material grains could be observed. The 3D surface analysis showed that a large fractal dimension was obtained for the stress amplitude τ_{an} in the range of higher loads, indicating the surface's high complexity. Analysing the isotropy of the surface using the Str parameter and assessing the percentage level of isotropy, it can be concluded that the obtained surfaces have a periodic anisotropic character, which proves that a structure subjected to high stresses has a directed and dominant direction of cracking.

Keywords: tin-zinc-lead bronze, cyclic torsion, torsion surface, surface topography, fractals.

INTRODUCTION

Fracture planes have been analysed for many years. These analyses are carried out broadly from various angles. Such analyses are performed regarding test conditions: monotonic, dynamics and fatigue. Fracture mechanics deals with a detailed analysis of these issues. In the case of fatigue, the loading method is important, particularly whether it is tension-compression, cyclic bending or cyclic torsion. Here, the crack surface and the directions of fatigue cracks are important.

The fatigue cracking process can be divided into three stages. The first stage is the initiation process, the second is propagation, and the last is monotonic (or dynamic) collapse. Depending on the load level and, consequently, on the fatigue

life, these surfaces and their proportions differ. This also applies to the directions of fatigue cracks.

Generally, materials can be divided into two types of fatigue cracks. The first type is material in an elastic-plastic state, where the initiation of cracks starts from one of the directions determined by the maximum shear stresses, and the second type, for materials in a brittle state, the initiation of fatigue cracks takes place in the direction of the maximum normal stresses. However, the propagation has exactly the opposite direction, i.e. in the first case in the direction of normal stresses [1–2], and in the second case in the direction of tangential stresses [1–4]. There are also materials in an intermediate state, meaning the crack directions are intermediate [5]. Most often, we deal with materials in an elastic-plastic

state. In this case, the maximum normal stresses generally determine the fracture surfaces.

In the case of tension-compression or pendulum bending, the position of the scrap plane is obvious and is defined by the maximum normal stresses. Examples of cracks are shown in Figure 1 for our own tests of RG7 bronze [6]. In the case of tension-compression, fatigue cracks can be seen developing from the outer surface towards the sample axis. In the case of pendulum bending, it can be seen that fatigue cracks develop from the two points with the highest stress amplitude and develop towards the bending plane, which is not a loaded plane. This surface is visible in the photo as a dark strip running through the entire cross-section. In both cases, the scrap surfaces are perpendicular to the sample axis. However, the matter is not so obvious in the case of cyclic torsion. The maximum stress occurs on the circumference and is zero at the axis of rotation. Bronze is a good material for outdoor structures because it does not rust in the same way as steel, which does not mean that it does not corrode. The oxidation process of bronze creates an oxide layer on its surface, the structure of which slows down the process. In the case of cyclic torsion, the fracture planes are not

as evident as in the case of tension-compression or cyclic bending. Even before the monotonic fracture of the sample, various directions of fatigue cracks can be observed on the sample surface. Figure 2 shows an example of such an overexposed sample 2a shows the entire sample, and Figure 2b shows its cross-section. Perpendicular cracks can be observed, appearing perpendicularly along the sample, so they later develop at an angle of 45°.

In paper [7], it was shown that the directions of cracks for torsion of titanium alloy samples initiate in the direction of the maximum shear stresses normal along the axis or perpendicularly and then propagate along the direction defined by the maximum normal stresses, i.e. at an angle of 45 or in two directions (type X) also at an angle of 45. It was noticed that [8], in the case of large loads with variable torque, cracks develop along the maximum tangential directions in the direction coinciding with the axis of the sample, and in the case of smaller loads, at an angle of 45. However, no differences were noticed for a variable axial load.

It was noticed [9] that in the case of rapid growth of fatigue cracks, i.e. for high loads,



Figure 1. Classic fatigue crack surfaces after tensile-compressive and pendulum bending tests and RG7 bronze with a diameter of 10 mm at the narrowing point

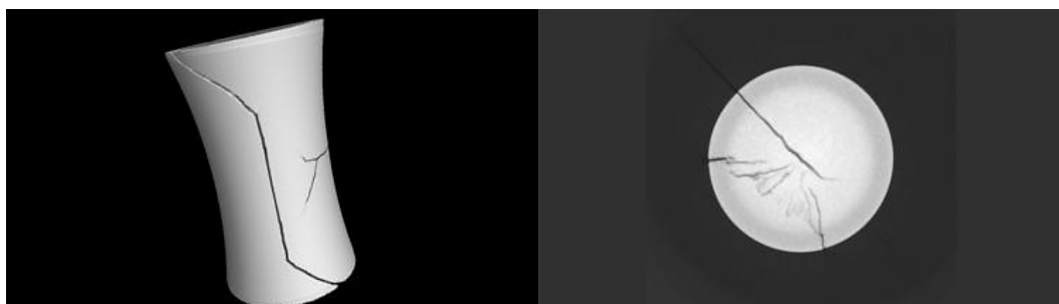


Figure 2. Example of an overexposed RG7 bronze sample after cyclic twisting: (a) the entire sample, (b) a cross-section of the sample

cracking occurs according to model I, and in the case of lower loads it is a mixed model of fatigue crack propagation.

In the case of cyclic twisting of copper [10], it turned out that for small shear stress amplitudes of 75 MPa and 90 MPa, the fatigue crack surfaces are smooth, while for larger ones (100 MPa and 150 MPa), they are jagged and with faults parallel to the sample axis. Similar properties were observed in paper [11] when testing A357-T6 cast aluminium alloy. Here, for the highest stresses, the macroscopic fracture surface for the highest shear stress amplitudes coincides with the direction determined by the maximum shear stresses and is perpendicular to the surface.

In the case of cyclic torsion of 100C6 bearing steel [12], the place of initiation of a fatigue crack depends on the load level, i.e., in effect, on the fatigue life. Generally, fatigue crack initiation occurs on the sample surface for shorter durability. However, cracking begins on the external surface and inside the material for loads in the gigacycle range. According to the authors, this is due to inclusions that cause local stress concentration, which causes greater elastic-plastic stresses than shear stresses resulting from torsion.

Based on fatigue tests on copper [13], it was found that the fatigue strength exponent b_0 (fatigue strength exponent) increases with the increase in the fatigue strength coefficient τ'_f (fatigue strength coefficient). This is exactly the opposite of the tension-compression case.

In [14], the influence of initial twisting on the cracking direction was demonstrated based on fatigue tests with cyclic twisting of samples made of 45CrMoVA steel. It was shown that this angle is increasingly smaller from 51.11° to 44.50° as the initial twist angle increases from 8.3° to 16.3° . According to the torsional fatigue characteristics described in the literature [15–17], the fracture patterns of the samples can be roughly divided into two types. One is NF and TS (transversal shear fracture) mixed mode (NTF), and the other belongs to NF (normal stress fracture), LS (longitudinal shear fracture) and TS mixed mode (NLTF). The NTF surface consists of crack initiation, crack propagation and final crack zones, which is characteristic of smaller initial twist angles. However, for larger initial twist angles we are dealing with a mixed NLTF mode, the initiation, propagation and final fracture zones correspond. The NTF model comprises crack initiation, propagation, and terminal crack zones. The

fatigue crack initiation site is at the surface, suggesting that fatigue crack initiation occurs mainly influenced by the maximum normal stress. This indicates that the propagation of fatigue cracks in area II is mainly dominated by pure shear stress. The maximum normal stress also caused the initial fracture of the NLTF. The crack propagated along AD and the radial direction (RD) under pure shear stress. Due to a shear stress gradient, the shear stress gradually decreases along the RD, and the crack propagation along the RD dominated by the shear stress will be hindered after travelling a certain distance inward.

Tests of steel 4340 [18] under cyclic torsion showed that the initiation of fatigue cracks occurs in accordance with the tangential stress perpendicular to the outer surface. Then, at a certain distance from the surface, microcracks appear from shear stresses perpendicular to the surface and parallel to the axis. These cracks then coalesce, resulting in a macroscopic crack at an angle of 45° , which coincides with the maximum normal stress. Therefore, a more complete analysis of the fracture surfaces is necessary, as this approach may lead to erroneous conclusions.

When analysing the directions of fatigue cracks, however, one must remember that the directions of fatigue crack initiation, the macroscopic directions of fatigue cracks and the locations of critical planes used in the case of applying the multiaxial fatigue criteria are different [19–21]. Recently, they are increasingly used in many models when dealing with a multi-axial load condition to generalise these criteria [22] or propose new ones [23]. It also turns out that it is possible to apply the criteria in the critical plane for composite materials [24]. However, in [25], the analysis of the location of the critical plane with the fatigue crack initiation planes was performed for testing St52-3N steel.

In the literature, one can find numerous works dealing not only with fatigue life, but also with fatigue crack surface, topography, and fractal description. However, these analyses mainly concern tension-compression, less frequently pendulum bending. However, such descriptions for cyclic torsion can be found very rarely. Few works concern this phenomenon for fatigue tests in these conditions for steel [26–28]. However, in the work [27], this problem was taken up not only for steel but also for the copper alloy CW008A. Therefore, undertaking attempts to analyze

non-ferrous materials seems to be most relevant and necessary.

This paper aims to analyse fatigue cracks during cyclic torsion of samples made of RG7 bronze for various load levels. Fatigue crack surfaces will be analysed in terms of their orientation and 3D surface analysis of fractal dimension and surface isotropy using the Str parameter.

MATERIAL AND RESEARCH

Fatigue tests were performed on samples made of RG7 tin-zinc-lead bronze. This material is also known as CuSn7Zn4Pb6 (DIN), CC493K (EN), 2.1090 (DIN WN), B746 (PN). The material was supplied in the form of drawn bars of 16 mm diameter. The basic mechanical properties are presented in Table 1. Detailed research results were presented in previous paper [6].

These tests were carried out with cyclic torsion with a controlled torque amplitude, up to a

30% drop in stiffness, i.e. an increase in lever deflection, on “diabolo” samples with a diameter of 10 mm and a station presented in detail in [29]. Figure 3 shows a diagram of the test stand and a drawing of the sample used in the tests.

Table 2 lists the results of these tests ordered by stress amplitude. According to the elastic-plastic model presented in [6], the amplitudes of shear stresses and the corresponding amplitudes of shear strains were determined for torsion. The values of the nominal stress amplitudes and for the elastic-plastic model are shown in Table 2.

The nominal stress amplitude value was determined based on

$$\tau_{an} = \frac{M_{ta}}{w_o} \tag{1}$$

where: M_{ta} is the value of the set torque amplitude.

Additionally, the amplitudes of specific strains were determined and are included in this table and in Figure 4a, where the deformation fatigue characteristics are plotted. It can be seen

Table 1. Basic static properties of the tested materials

Material	$\sigma_{u(min)}$, MPa	$\sigma_{y(min)}$, MPa	$A_{50mm(min)}$, %	E, GPa	u
RG7	270	120	15	92.14	0.3

Note: A – area of cross-section.

Table 2. Tests of RG7 bronze under cyclic symmetric torsion conditions

Sample	τ_{an} , MPa	τ_{aep} , MPa	γ_{aep}	N_{exp} , cycles
012	102	79	2.588	> 10000000
030	115	90	3.063	3215695
020	117	92	3.154	1349697
024	117	92	3.154	3021316
029	125	98	3.439	742896
033	125	98	3.439	2499155
004	127	100	3.537	650800
021	127	100	3.537	481710
038	135	107	3.898	289812
039	135	107	3.898	785924
006	143	113	4.227	70400
028	143	113	4.227	19122
018	143	113	4.227	86055
007	153	121	4.699	171275
011	153	121	4.699	93219
040	158	126	5.013	35902
041	158	126	5.013	3215
019	163	130	5.275	17271

Note: γ_{aep} – elasto-plastic shear strain, N_{exp} – Experimental number of cycles.

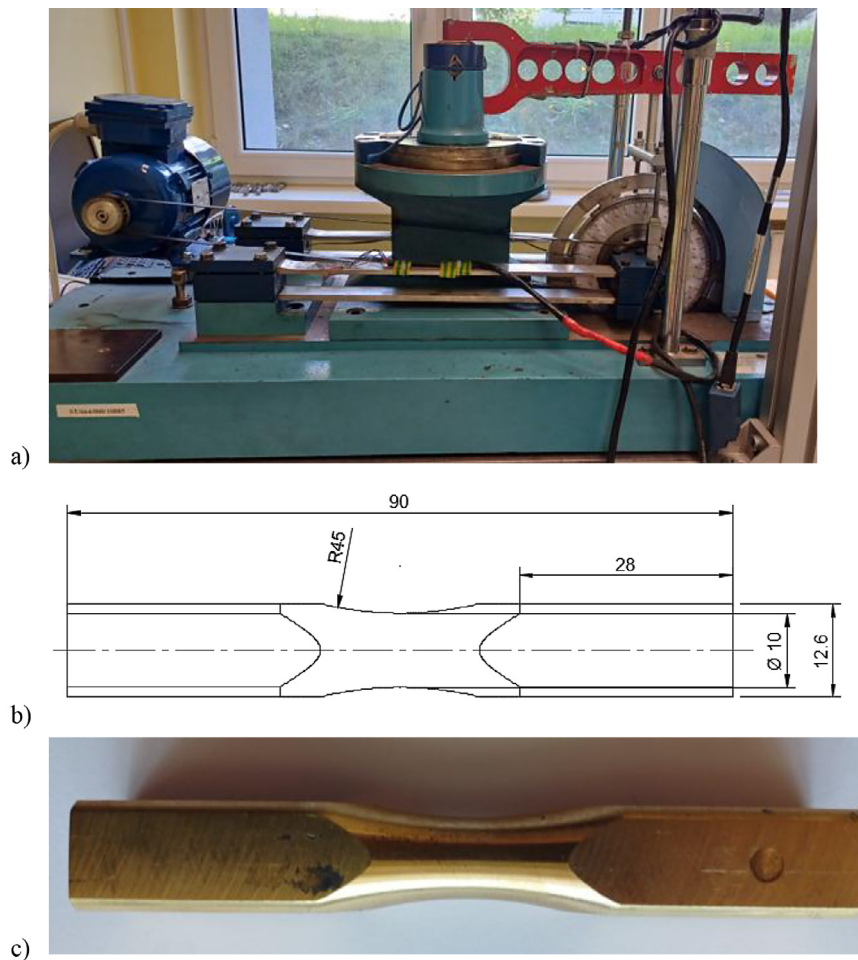


Figure 3. (a) Schematic diagram of the test stand and (b) drawing of the sample and (c) photos

that this characteristic is a straight line in a double logarithmic system in a large durability range from 3.000 to 3,000,000 cycles, which is not typical for deformation characteristics.

FRACTOGRAPHIC ANALYSIS OF FATIGUE FRACTURES

Figure 3b shows macroscopic photos of cracked samples, indicating the average macroscopic directions and angles of fatigue cracks. Selected photos showing marked crack angles are presented in detail in Figures 5–7.

Based on macroscopic SEM (scanning electron microscope) photos, it was found that at low-stress amplitudes, cyclic torsion of the analysed samples causes fatigue cracks in the samples at an angle of approximately 40° (Figure 4b, 5a). The fracture surfaces of samples observed in this system are relatively smooth (Figure 4b). At the same time, as the stress amplitude increases, the

value of the determined fatigue crack angles decreases significantly. A decreasing tendency was observed in correlation to the increasing value of stress amplitude (Figure 4b). Thus, with an amplitude of 158 MPa (Figure 5b), the determined fatigue crack angle is $26^\circ 44'$. It is worth noting that for the highest amplitude value (163 MPa, Figure 6), the fatigue crack angle was not determined, and the observed fracture surfaces of samples is jagged, with characteristic faults developing in different direction

Figures 7–15 shows macrophotographic images of the obtained fractures for selected samples, with characteristic fatigue areas marked, allowing for the distinction of individual stages of fatigue cracking. The observed fatigue fracture surfaces show significant differences depending on the applied load level.

The place where crack initiation occurs is an area of local stress concentration, perhaps caused by the presence of defects. For each analysed sample (Figures 7–15), the visible crack

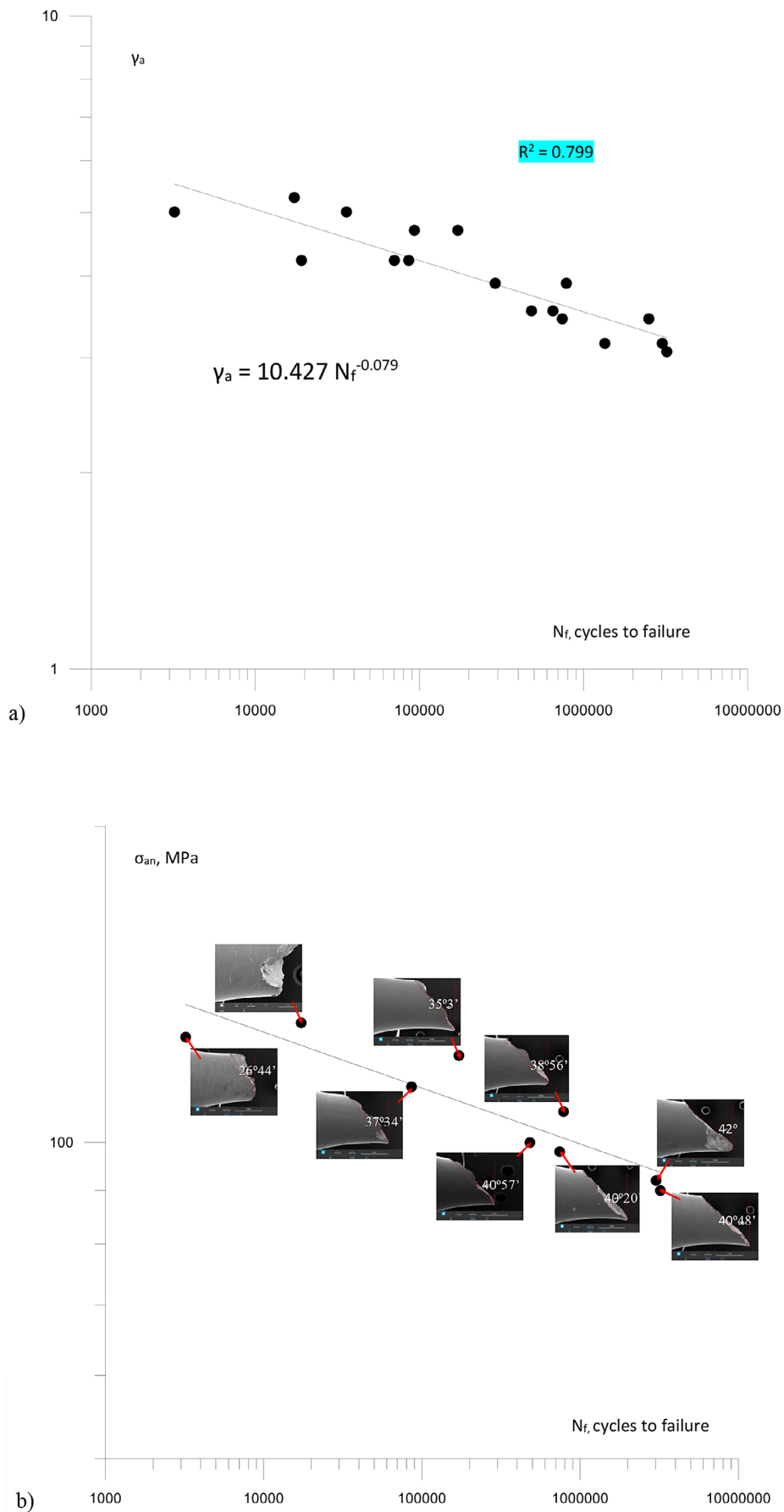


Figure 4. (a) Deformation fatigue behavior of RG7 bronze for cyclic torsion, and (b) stress fatigue characteristics with the given values of fatigue crack angles, (σ_{an} – nominal normal stress amplitude, γ_a – amplitude shear strain)

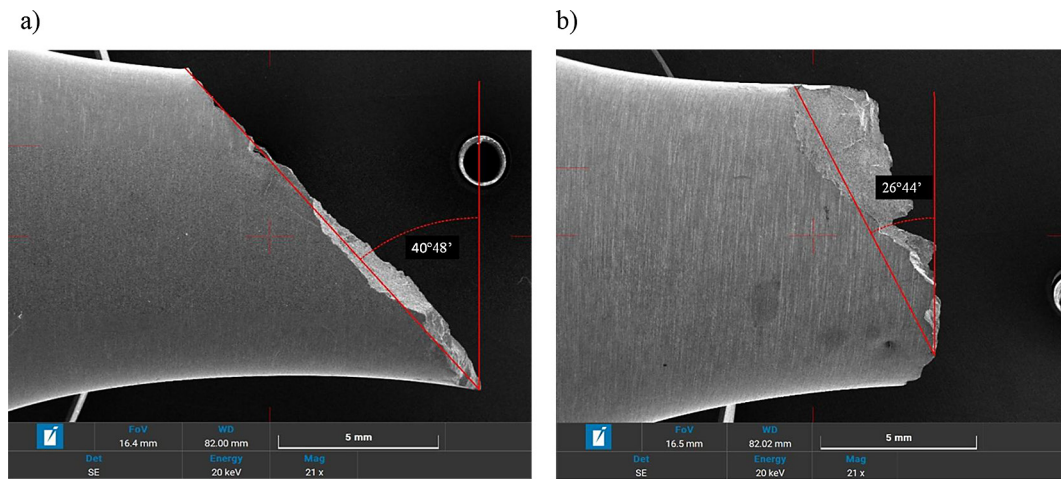


Figure 5. Fracture surface with the determined angle of the inclined fracture plane for the sample (a) 030; $\tau_{an} = 115$ MPa, (b) 041; $\tau_{an} = 158$ MPa, τ_{an} – nominal shear stress amplitude

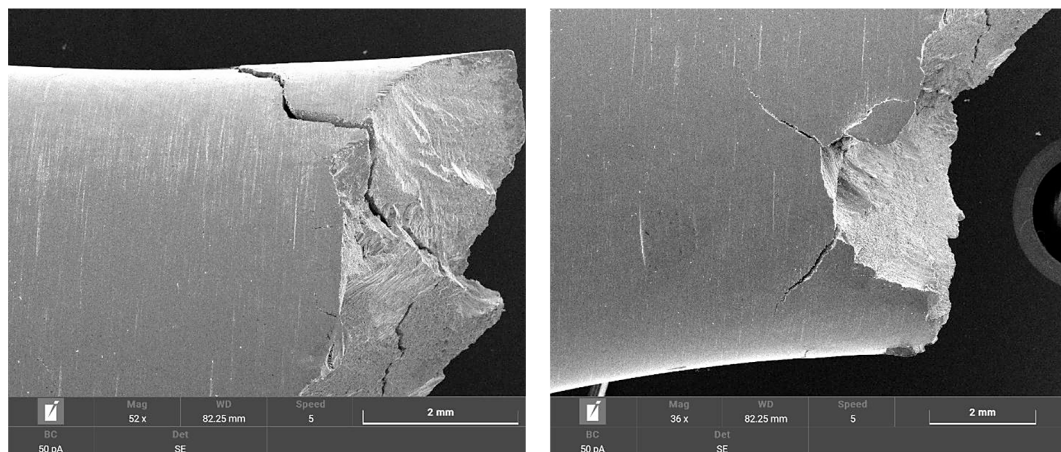


Figure 6. Fracture surface with the determined angle of the inclined fracture plane for the sample 019; $\tau_{an} = 163$ MPa

propagation zone is characterised by slight roughness, where clear beach marks can also often be observed (Figures 7–10).

For samples with the lowest stress amplitude value (Figures 7–9), the share of the fracture zone in relation to the crack propagation zone is small. The situation changes as the stress amplitude increases (Figures 10–15), where the observed surface is characterised by a proportionally larger share of the fracture zone. In the case of Figures 7–12, the crack propagation zone appears smooth at low magnification, which reflects the impact of a low-amplitude stress load on the element.

The situation is completely different in the case of high amplitude (Figures 13–15). Here, this area is characterised by the presence of irregularities, and along the edge of the crack initiation, secondary faults can be seen. In these two cases, the micro-relief of the topography is

similar throughout the area. Small irregularities, tears and cracks running deep into the surface of the scrap were noticed.

From the preliminary analysis of the crack surfaces, it can be seen that the share of the surface that is fatigue and fractured (monotonic) varies for different samples. This area, or more precisely the percentage, can be correlated with the fatigue life or the load amplitude. This was already noticed by Strzelecki for tension-compression [30] and rotating bending [31]. Figure 16 shows the relationship between the percentages of the fatigue cracking area and the entire surface, projected onto surfaces normal to the sample axis.

$$P = \frac{A_f}{A} \times 100\% \quad (2)$$

where: P – percentages of the fatigue cracking area, A_f – fatigue area of cross-section.

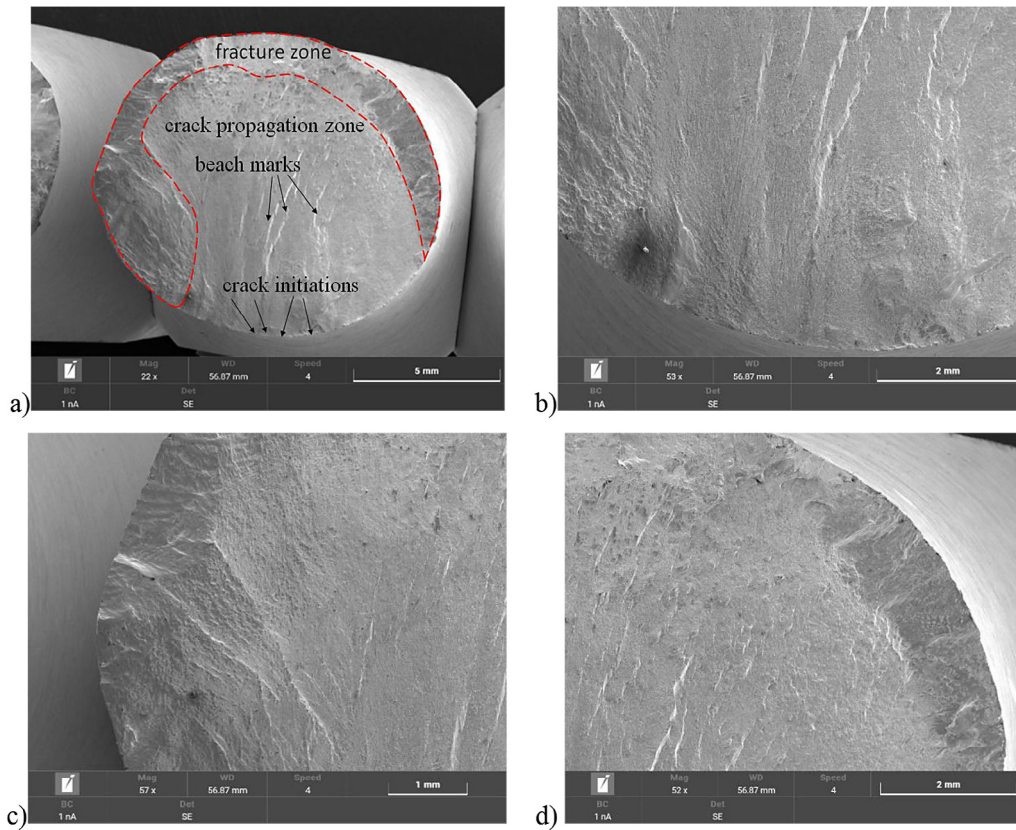


Figure 7. Fracture surface morphology (a); crack initiation zone (b); fracture zone (c-d) of sample 030;
 $\tau_{an} = 115 \text{ MPa}$

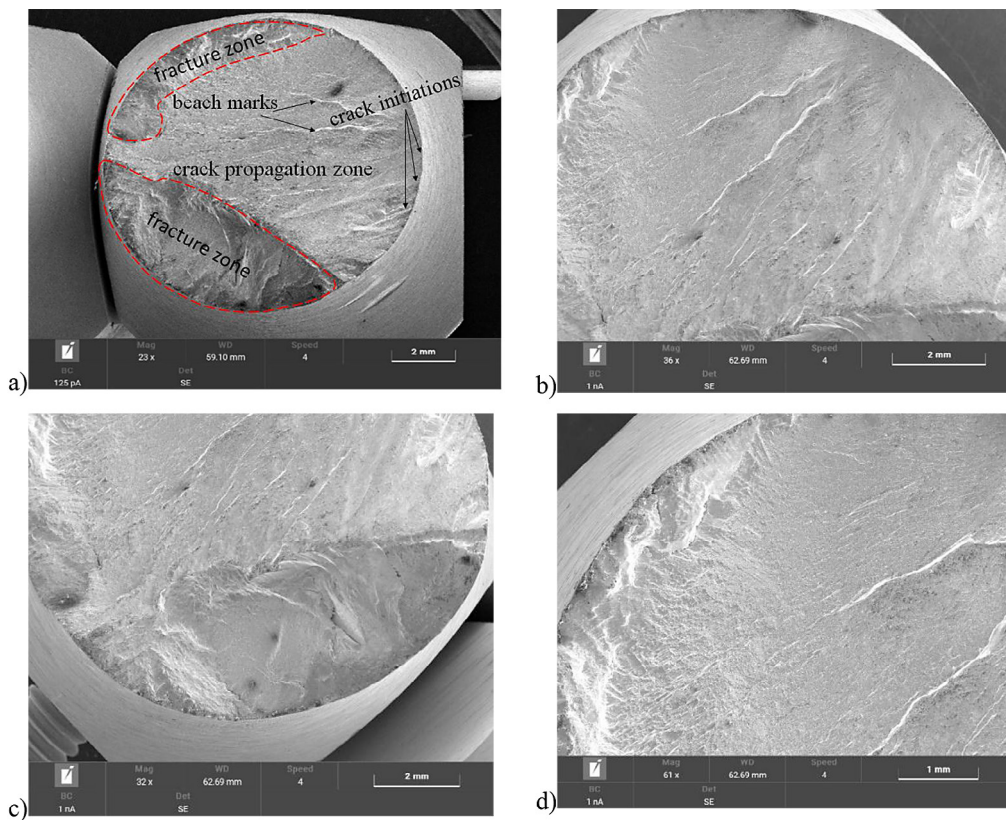


Figure 8. Fracture surface morphology (a); crack initiation zone (b); fracture zone (c-d) of sample 024;
 $\tau_{an} = 117 \text{ MPa}$

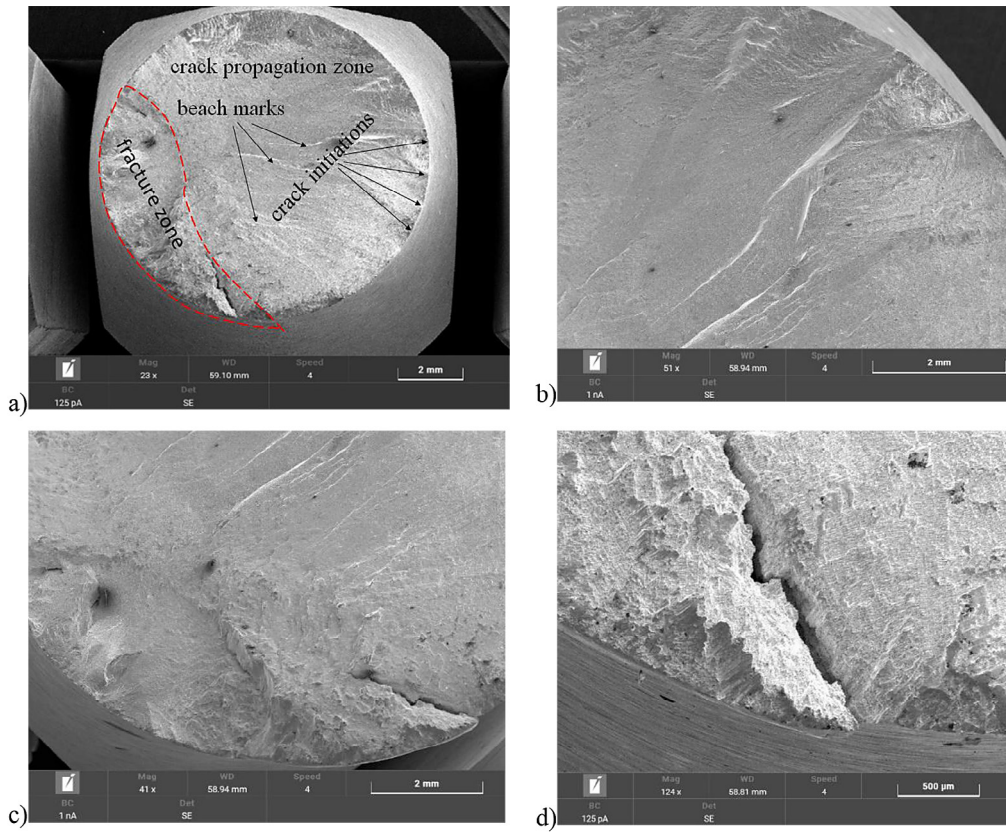


Figure 9. Fracture surface morphology (a); crack initiation zone (b); fracture zone (c-d) of sample 029; $\tau_{an} = 125$ MPa

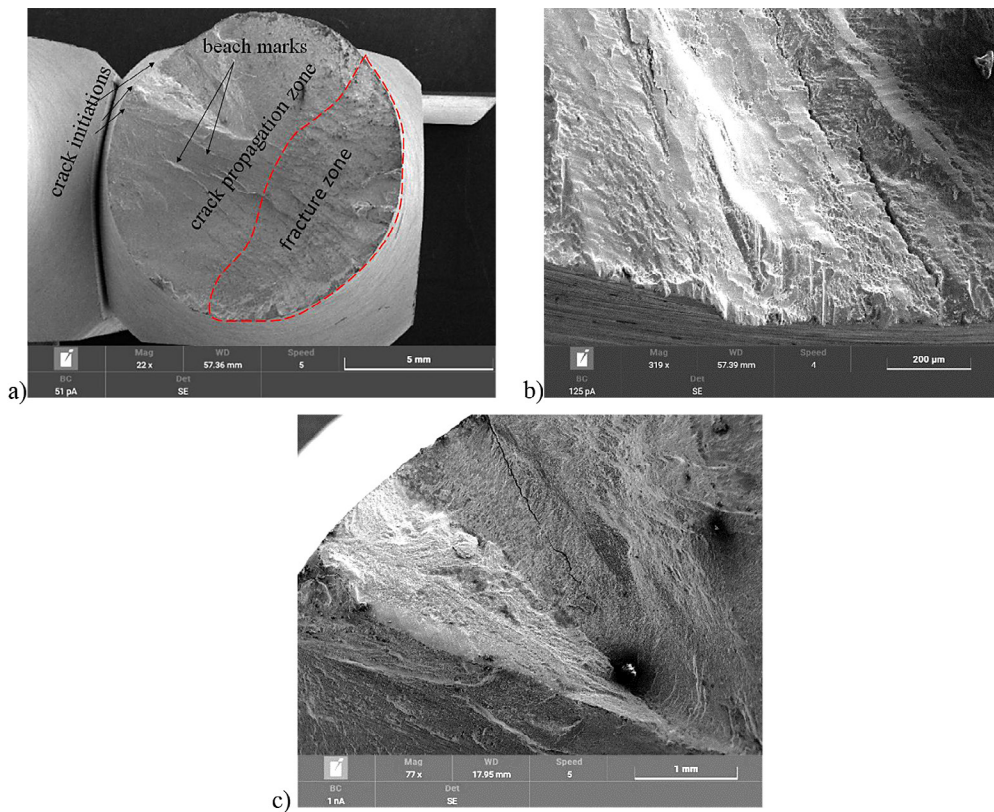


Figure 10. Fracture surface morphology (a); fracture zone (b); crack propagation zone (c) of sample 021; $\tau_{an} = 127$ MPa

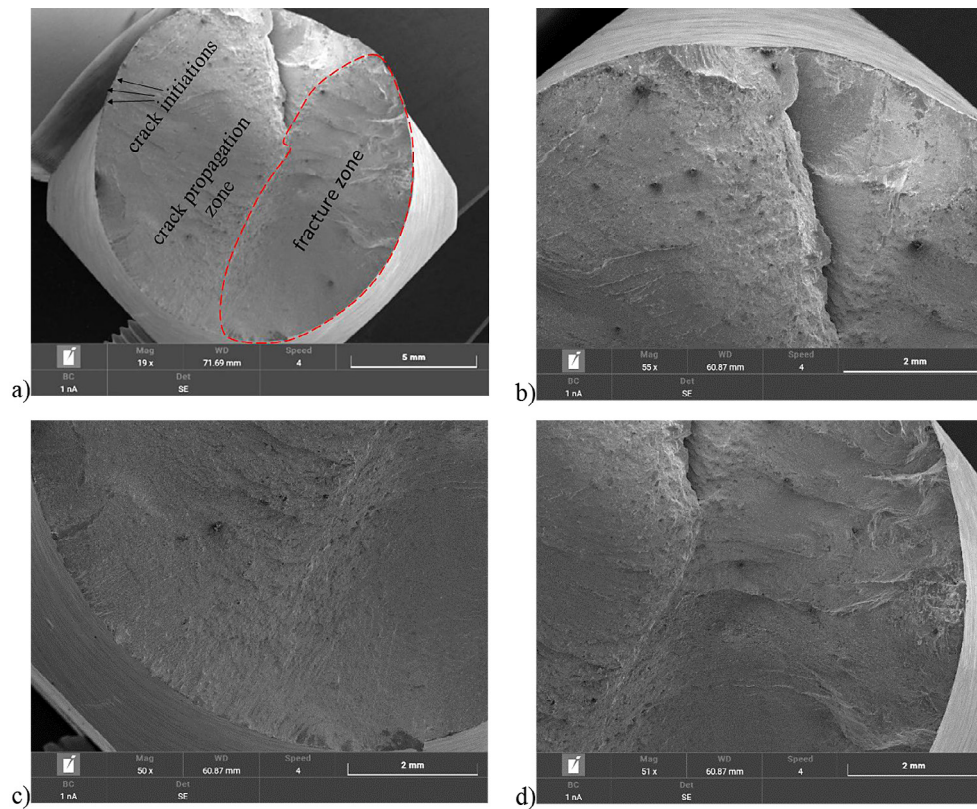


Figure 11. Fracture surface morphology (a); crack propagation zone (b-c); fracture zone (d) of sample 039;
 $\tau_{an} = 135 \text{ MPa}$

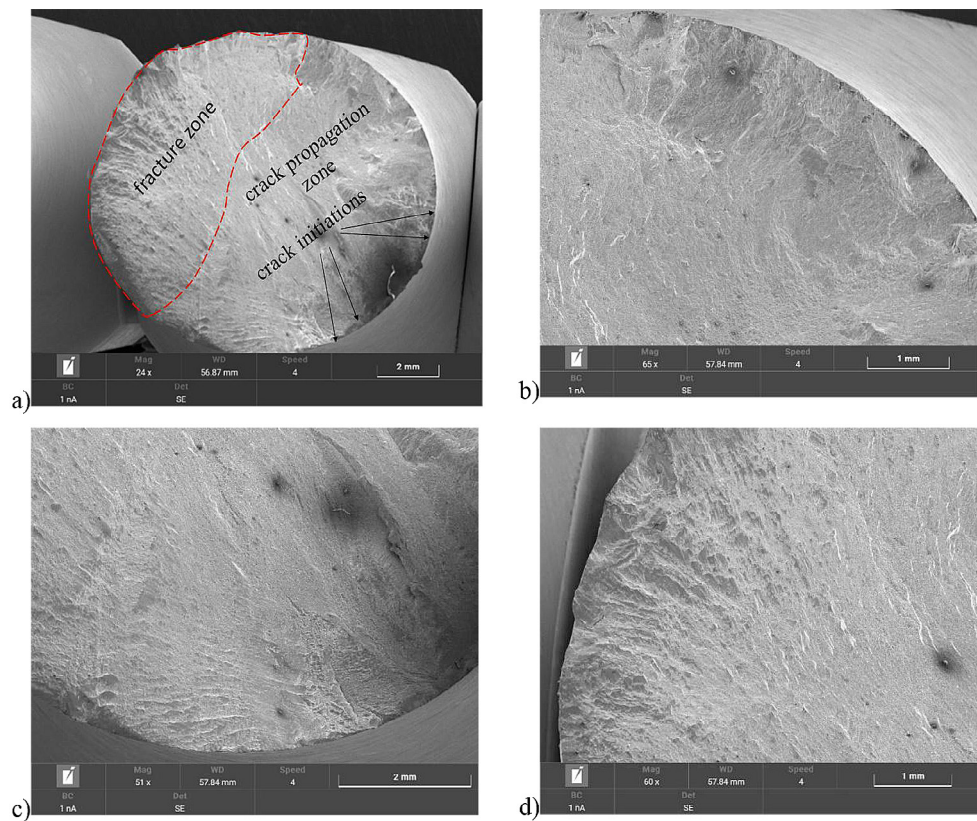


Figure 12. Fracture surface morphology (a); crack propagation zone (b-c); fracture zone (d) of sample 018;
 $\tau_{an} = 143 \text{ MPa}$

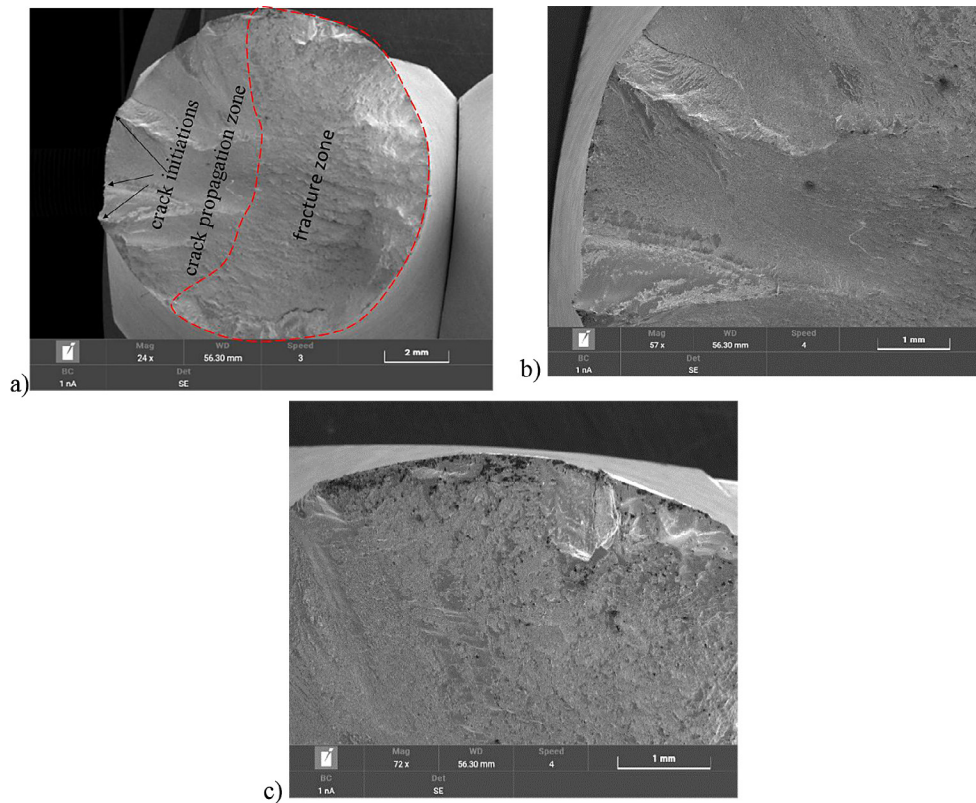


Figure 13. Fracture surface morphology (a); crack propagation zone (b); fracture zone (c) of sample 007; $\tau_{an} = 153 \text{ MPa}$

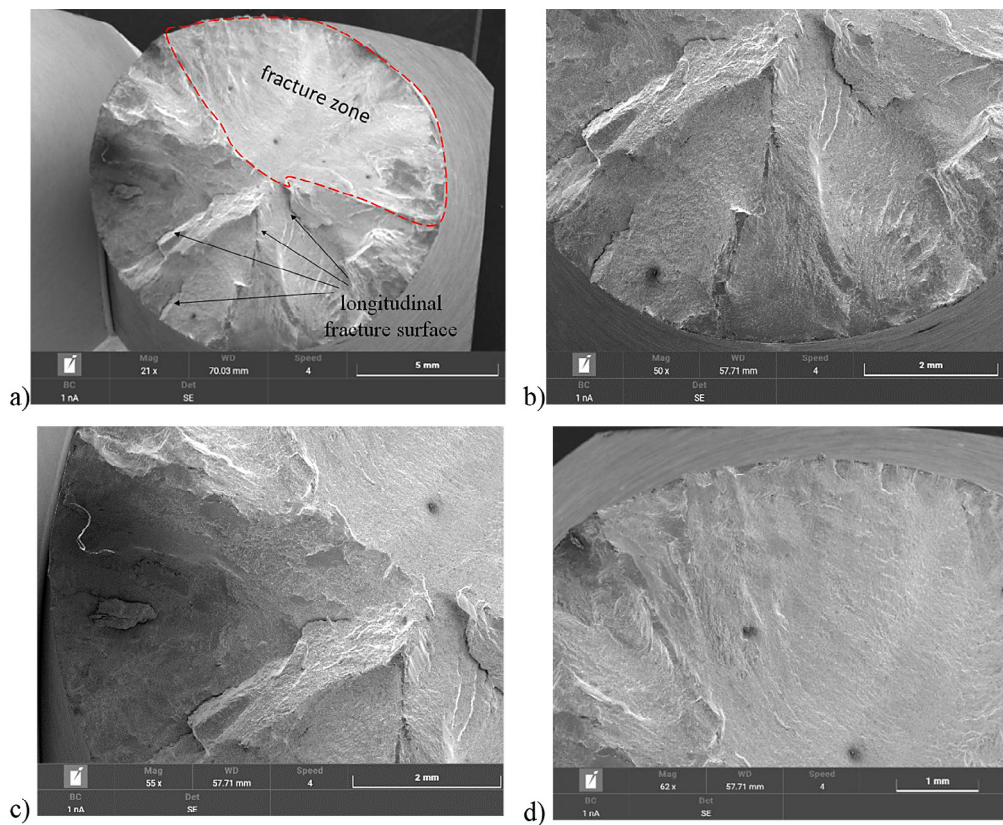


Figure 14. Fracture surface morphology (a); crack propagation zone with longitudinal fracture surface (b-c); fracture zone (d) of sample 041; $\tau_{an} = 158 \text{ MPa}$

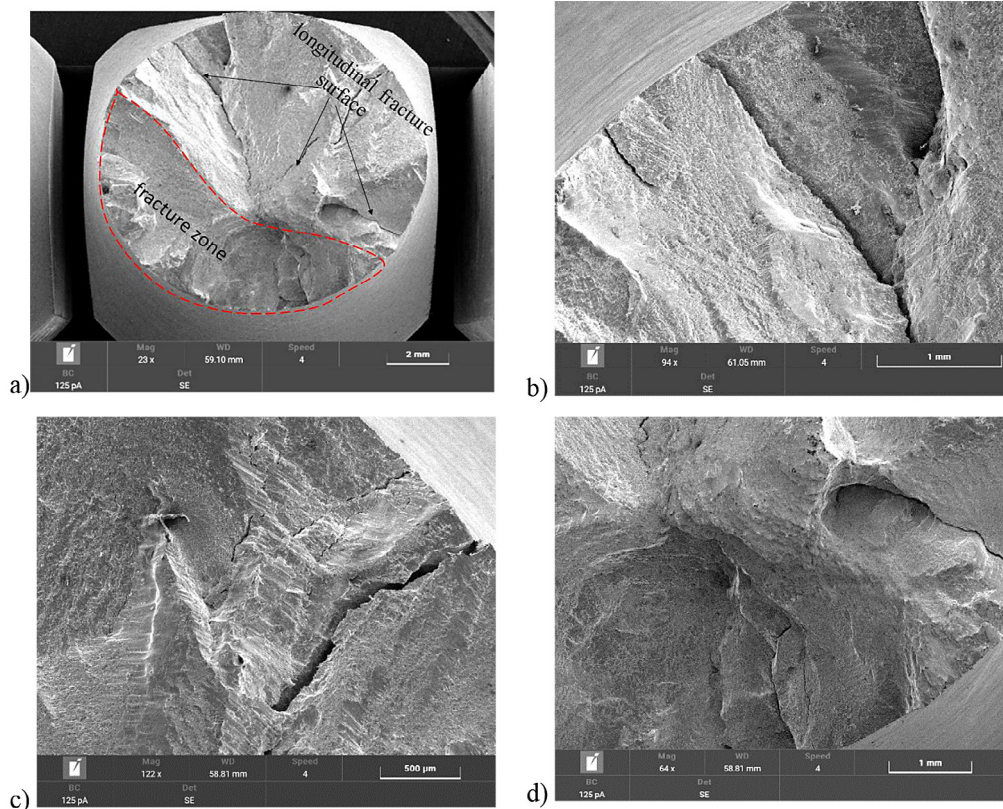


Figure 15. Fracture surface morphology (a); crack propagation zone with longitudinal fracture surface (b-d) of sample 019; $\tau_{an} = 163$ MPa

Figure 16a shows the relationship as a function of durability in the form:

$$P = 108.79 - 4.92 \log N_f \quad (3)$$

where: N_f – cycles to failure.

a in Figure 16b as a function of shear stress amplitudes according elasto-plastic model

$$P = 0.82 \tau_{aep} - 40.91 \quad (4)$$

From the analysis of the drawings it can be observed that in both cases there is a linear relationship. However, in the case of durability dependence, the logarithm of durability is on the ordinate axis. It can be seen that as the stress amplitude increases, i.e. lifetime decreases, the percentage of the surface damaged due to fatigue increases.

TOPOGRAPHIC ANALYSIS OF FATIGUE FRACTURES

When analysing surface fractures, the first focus was on fractal analysis. This is because geometric fractals have features or forms that can be repeated in different sizes and scales, and an example of such repeatability of features in different

ranges of the room can be Koch curves or Minski sausage (curve) [32]. In other words, fractals can be used to search for behavioural patterns and describe surface complexity. Fractals can take dimensions that are not natural numbers and fractional values. It is assumed that the values obtained between 1 and 2 correspond to two-dimensional (2D) analysis, while values from 2 to 3 correspond to three-dimensional (3D) analysis. In the case of fractals with integer values equal to 3, we are dealing with volumetric analysis [33]. To determine the fractal dimension, the scale-dependent fractal analysis method was used, in which the analysis is based on the calculation of relative length or relative area as a function of scale (patchwork method). Measurements were repeated three times, and the presented results are averaged.

Figure 17a shows an example of a chart generated in the Mountains Map software to calculate the scale- and area-dependent fractal dimension for sample 030.

This method is used to quantify and model various phenomena whose geometric complexity may depend on scale and was developed by Professor Christopher Brown of Worcester

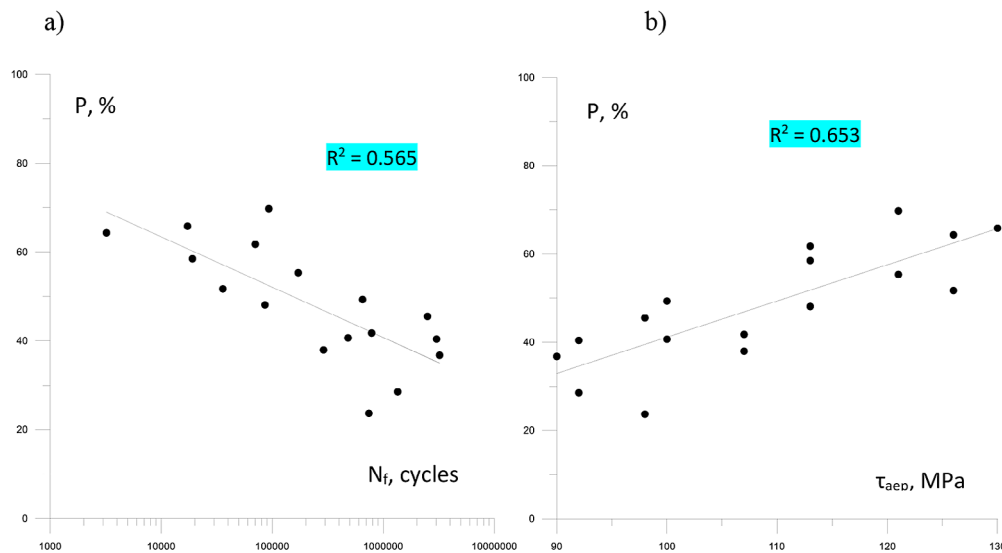


Figure 16. Dependence of the percentages of the fatigue cracking area to the entire surface P as a function of a) durability, b) shear stress amplitude

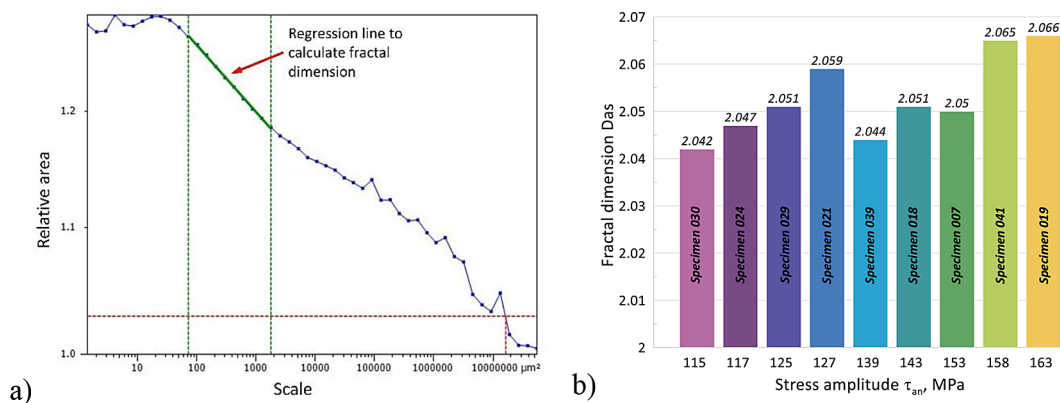


Figure 17. (a) sample chart for sample 030 to determine fractal dimensions using the scale-dependent fractal analysis method, (b) changes in the fractal dimension for the analyzed cases

Polytechnic Institute (WPI) [34–35]. This method uses triangular patches to estimate area as a function of the area of a single patch. Such a field is interpreted as the scale of observation or the scale of influence of morphology-dependent phenomena. This method identifies the so-called transition points or scale threshold for a given surface as well as facilitates the determination of the surface complexity parameter and can support the analysis of surface phenomena. In this method, the fractal dimension D is extended by the index as , which indicates that it is a fractal dimension derived from surface scale analysis [36].

Fractal analysis and other analyses were performed in the Mountains Map v 10 software by Digital Surf. Unfiltered surfaces were analysed because filtration of this type of surface may

result in dimensional distortion and falsification of measurement results.

The highest values of the fractal dimension, as shown in Figure 16b, were obtained for samples 021, 041, and 019, while for samples 041 and 019 for stress amplitudes nominal (shear stress amplitude) $\tau_{an} = 158$ and 163 MPa, the fractal dimension was the largest and amounted to (fractal dimension) $Das = 2.065$ and 2.066 , respectively. Large fractal dimension values for these fractures indicate their high complexity compared to other surfaces, which can be observed in Figure 18 of the surface after scanning with the 3D S neox optical profilometer from Sensofar (x-y dimension of the measured crack areas for all analyzed surfaces was 13.4×10.6 mm). For the surfaces after twisting, a characteristic deformation of the surface

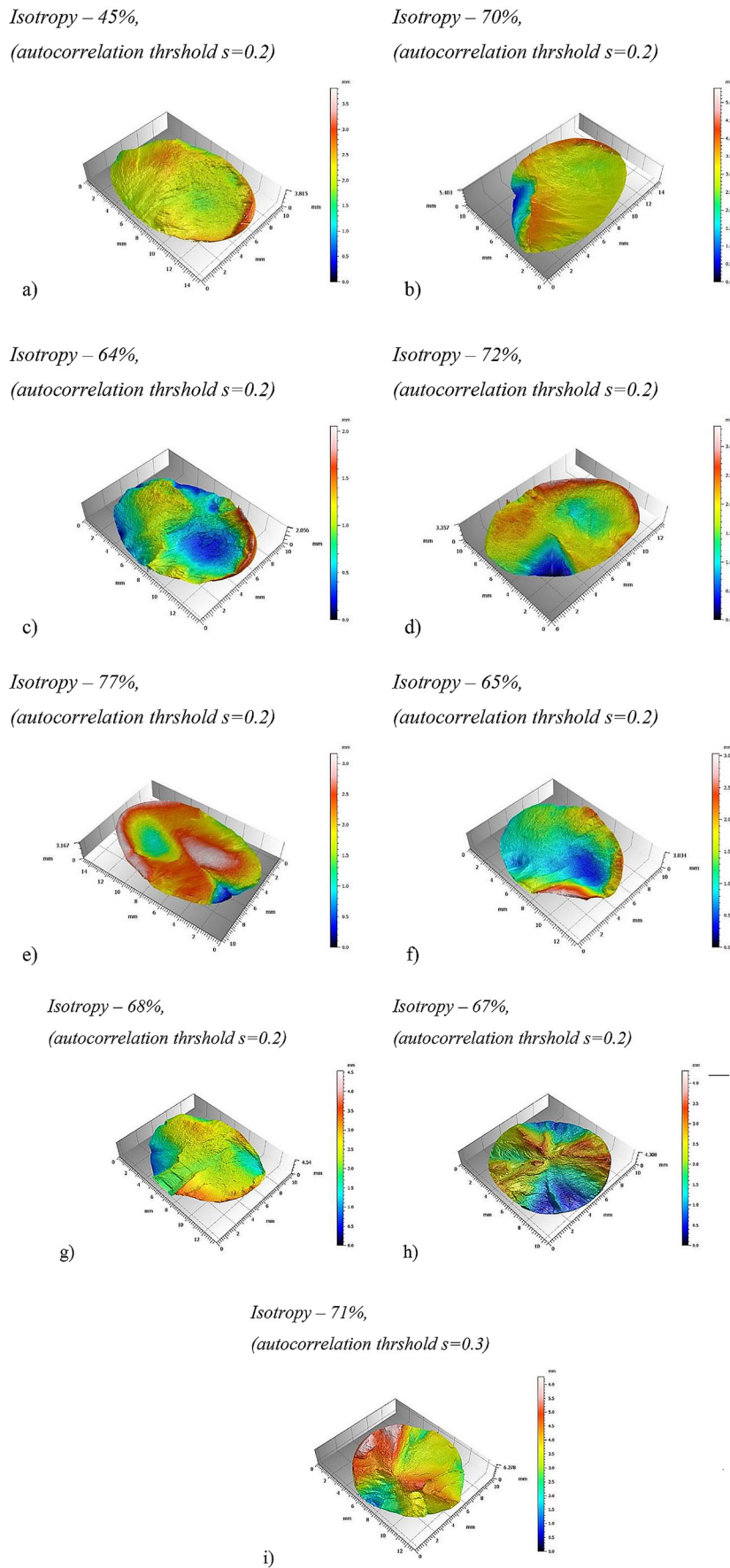


Figure 18. Examples of 3D views of the surface after scanning on the 3D S neox optical profilometer by Sensofar for samples: (a) 030; (b) 024; (c) 029; (d) 021; (e) 039; (f) 018; (g) 007; (h) 041; (i) 019

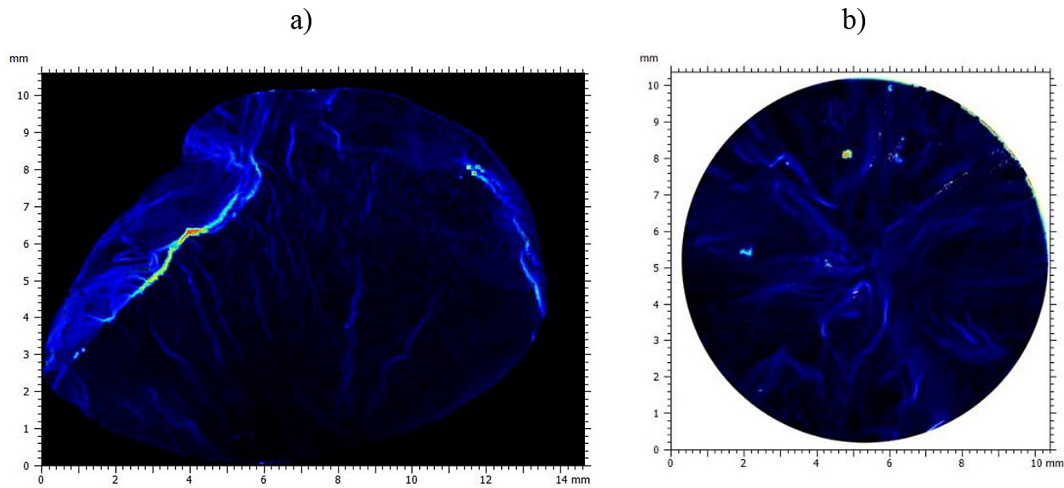


Figure 19. Local property maps: (a) sample 024; (b) sample 041

can also be observed, one of the reasons for which may be the influence of the temperature occurring during the twisting tests, which may result in material flow and small cracks without visible development, visible on the surfaces of Figure 18 and Figures 7–15 for smaller stress amplitudes. A stabilised course characterises the twist of samples 030-007, the appearance of which can be assessed as uniform (directed) without any significant special features, and the difference between the largest and the smallest value of the fractal dimension is approximately 0.83%. An example of such a course of uniform (directed) cracking is shown on the local property map, thanks to which it is possible to detect the complexity of the surface (Figure 19a) for sample 024. However, for samples with the highest stress amplitudes τ_{an} (sample 007-019), the torsion process is multidirectional, characterised by many branches but with dominant directions. An example of such multidirectional

cracking is sample 041, also shown in the local property map of Figure 19b.

Figure 20a shows the change in the Str parameter (texture aspect ratio) for the analysed surfaces after twisting. Thanks to this parameter, we can assess the isotropic or anisotropic nature of the surface. Str ranges from 0 to 1, where values close to 0 are surfaces showing anisotropy (the surface then has a dominant direction), while when Str is close to 1, we are dealing with isotropic surfaces (surfaces having the same properties regardless of the direction). An example of such a surface division for the Str parameter is shown in Figure 20b. All analysed surfaces are periodically anisotropic surfaces, as evidenced by the obtained parameters Str (Figure 20a). This fact is also confirmed by the percentage of surface isotropy, which for most cases was in the range of approximately 60–70%. On average, it gave a result of 66%. and did not exceed the 80% threshold.

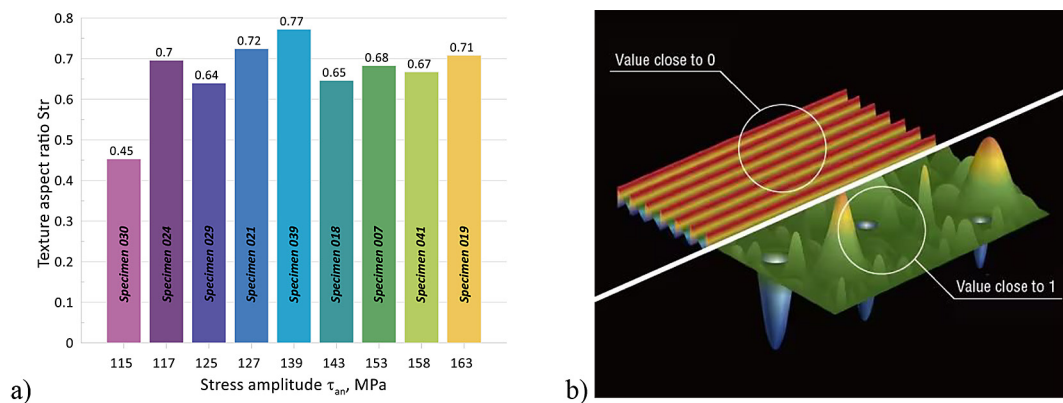


Figure 20. Str parameter for all analysed surfaces (a), assessment of isotropic and anisotropy of the surface (b) [33]

Above the 80% threshold, we are dealing with isotropic surfaces [37]. However, this value was much smaller for one case (the lowest load) and amounted to only 45%.

CONCLUSIONS

The analysis of the tests performed showed that:

1. The deformation fatigue characteristic for torsion is a straight line in a double logarithmic system over a large range of durability. Fatigue tests during cyclic torsion were characterized by relatively large scatter – R^2 coefficient is 0.799.
2. Load levels determine the direction of fatigue cracks for cyclic torsion. For lower loads, the macroscopic surface of fatigue cracks is inclined at an average angle of 40° (42° , $40^\circ 48'$, $40^\circ 20'$, $40^\circ 57'$). The angle of the inclined plane of a torsion fatigue crack tends to decrease with increasing stress amplitude. For higher loads, it is characterised by a decrease in the value of the surface inclination angle ($38^\circ 56'$, $37^\circ 34'$, $35^\circ 3'$, $26^\circ 44'$), because in the final stage of cracking faults appeared propagating in different directions.
3. On the surface of fractures obtained from fatigue tests, fracture zones and crack initiation zones of various sizes can be distinguished. The greater the loads the samples were subjected to, the more difficult it was to distinguish the boundary between these zones in the fracture structure.
4. The lower the load carried by the tested samples, the more uniform the appearance of the fracture surface. In the case of samples tested at lower stresses, a fracture zone was observed in the lower part of the fracture, which was damaged in the final stage of the test. This part of the fracture was characterised by a rougher surface, where tearing of material grains could be observed. The analysis of selected breakthroughs reveals the edge separating characteristic zones. The crack initiation areas were located in the top layer. Several crack initiation sites were observed in all samples. In the case of a large stress amplitude, microcracks of significant dimensions appeared in the vicinity of the sample perpendicular to the edge.
5. The percentage of the fatigue crack area to the total crack area can be described by a linear

function concerning the logarithm of lifetime or the shear stress amplitude resulting from cyclic torsion. In this case the R^2 coefficients are 0.565 and 0.653, respectively.

6. The analysis of the 3D surface showed that the large fractal dimension obtained for the stress amplitude τ_{an} in the range of 153–163 MPa indicates the high complexity of the surface. For this load level, correspondingly lower fatigue lives were obtained
7. Analyzing the isotropic of the surface using the Str parameter, which is on average 0.66, and assessing the percentage level of isotropy, it can be concluded that the obtained surfaces have a periodic anisotropic character, which proves that the structure subjected to high stress has a directed and dominant direction of cracking.

Acknowledgments

This paper was financially supported by the Opole University of Technology as part of the GRAS project no. 256/23.

REFERENCES

1. Brown M.W., Miller K.J. Initiation and growth of cracks in biaxial fatigue, *Fatigue and Fracture of Engineering Materials and Structures* 1979; 1, <https://doi.org/10.1111/j.1460-2695.1979.tb00380.x>
2. McDiarmid D.L. Fatigue under out-of-phase biaxial stresses of different frequencies. *Multiaxial Fatigue*. ASTM STP 853. In: K.M. Miller, M.W. Brown, editors. 1985; 606–621.
3. Fatemi A., Socie D.F. A critical plane approach to multiaxial fatigue damage including out-of-phase loading. *Fatigue and Fracture of Engineering Materials and Structures* 1988; 11, <https://doi.org/10.1111/j.1460-2695.1988.tb01169.x>
4. Socie D.F. Multiaxial fatigue damage models, *Journal of Engineering Materials and Technology, Transactions of the ASME* 1987; 109(4).
5. Nishihara T., Kawamoto M. The strength of metals under combined bending and torsion with phase difference. *Memories of the College of Engineering, Kyoto Imperial University* 1945; 11: 85–112.
6. Małeczka J., Łagoda T. Fatigue and fractures of RG7 bronze after cyclic torsion and bending. *International Journal of Fatigue* 2023; 168, <https://doi.org/10.1016/j.ijfatigue.2022.107475>
7. Nikitin A., Palin-Luc T., Shanyavskiy A., Bathias C. Comparison of crack paths in a forged and extruded

- aeronautical titanium alloy loaded in torsion in the gigacycle fatigue regime. *Engineering Fracture Mechanics* 2016; 167, <https://doi.org/10.1016/j.engfracmech.2016.05.013>
8. Gryguć A., Behraves S.B., Jahed H., Wells M., Williams B., Sud X. Multiaxial fatigue and cracking orientation of forged AZ80 magnesium alloy. *Procedia Structural Integrity* 2020; 25, <https://doi.org/10.1016/j.prostr.2020.04.055>
 9. Fonte M., Reis L., Romeiro F., Li B., Freitas M. The effect of steady torsion on fatigue crack growth in shafts. *International Journal of Fatigue* 2006; 28: 5–6, <https://doi.org/10.1016/j.ijfatigue.2005.06.051>
 10. Li R.H., Zhang P., Zhang Z.F. Torsional fatigue cracking and fracture behaviors of cold-drawn copper: effects of microstructure and axial stress. *Acta Metallurgica Sinica (English Letters)* 2019; 32, <https://doi.org/10.1007/s40195-019-00965-5>
 11. Serrano-Munoz I., Shiozawa D., Dancette S., Verdu C., Buffiere J.Y. Torsional fatigue mechanisms of an A357-T6 cast aluminium alloy. *Acta Materialia*. 2020; 201, <https://doi.org/10.1016/j.actamat.2020.09.046>
 12. Xue H.Q., Bathias C. Crack path in torsion loading in very high cycle fatigue regime. *Engineering Fracture Mechanics* 2010; 77(11), <https://doi.org/10.1016/j.engfracmech.2010.05.006>
 13. Li R.H., Zhang Z.J., Zhang P., Zhang Z.F. Improved fatigue properties of ultrafine-grained copper under cyclic torsion loading. *Acta Materialia* 2013; 61(15), <https://doi.org/10.1016/j.actamat.2013.06.032>
 14. Chen J.Z., Zhang B., Song Z.M., Wang H.Y., Zhang G.P. Influence of pre-torsion angles on torsion fatigue properties of 45CrMoVA steel bars. *International Journal of Fatigue* 2020; 137, <https://doi.org/10.1016/j.ijfatigue.2020.105645>
 15. Zhizhong H., Yusheng W., Heping C., Lihua M. Mechanism map of torsional fatigue fracture. *Acta Metallurgica Sinica (English Letters)* 1991; 4(2).
 16. Tschegg E.K. Mode III and Mode I fatigue crack propagation behaviour under torsional loading. *Journal of Material Science* 1983; 18.
 17. Wang C.H., Miller K.J. The effect of mean shear stress on torsional fatigue behaviour. *Fatigue and Fracture of Engineering Materials and Structures* 1991; 14: 2–3, <https://doi.org/10.1111/j.1460-2695.1991.tb00659.x>
 18. Makabe C., Socie D.F. Crack growth mechanism in precracked torsional fatigue specimens. *Fatigue and Fracture of Engineering Materials and Structures* 2001; 24(9), <https://doi.org/10.1046/j.1460-2695.2001.00430.x>
 19. Karolczuk A. Plastic strains and the macroscopic critical plane orientations under combined bending and torsion with constant and variable amplitudes. *Engineering Fracture Mechanics* 2006; 73(12), <https://doi.org/10.1016/j.engfracmech.2006.02.005>
 20. Karolczuk A., Macha E. Selection of the critical plane orientation in two-parameter multiaxial fatigue failure criterion under combined bending and torsion. *Engineering Fracture Mechanics* 2008; 75(3–4), <https://doi.org/10.1016/j.engfracmech.2007.01.021>
 21. Karolczuk A. Non-local area approach to fatigue life evaluation under combined reversed bending and torsion. *International Journal of Fatigue* 2008; 30: 10–11, <https://doi.org/10.1016/j.ijfatigue.2008.01.007>
 22. Łagoda T., Głowacka K., Kurek A. Fatigue life of aluminium alloys based on shear and hydrostatic strain. *Materials* 2020; 13(21), <https://doi.org/10.3390/ma13214850>
 23. Łagoda T., Kurek M., Głowacka K. A formulation of the criterion for multiaxial fatigue in terms of complex number as proposed by Macha, *International Journal of Fatigue* 2020; 133. <https://doi.org/10.1016/j.ijfatigue.2019.105430>
 24. Głowacka K., Łagoda T. Application of multiaxial fatigue criterion on critical plane to determine lifetime of composite laminates. *Engineering Fracture Mechanics* 2023; 292, <https://doi.org/10.1016/j.engfracmech.2023.109644>
 25. Lopez-Crespo P., Moreno B., Lopez-Moreno A., Zapatero J. Study of crack orientation and fatigue life prediction in biaxial fatigue with critical plane models. *Engineering Fracture Mechanics* 2015; 136, <https://doi.org/10.1016/j.engfracmech.2015.01.020>
 26. Zieliński D., Podulka P., Jiang C.-P., Macek W. Comparative assessment of entire bending-torsion fracture surface for 10HNAP steel using different optical measurement techniques, *Advances in Science and Technology Research Journal*, 2025; 19(6): 267–274, <https://doi.org/10.12913/22998624/202668>
 27. Walczuk-Gągała P., Pater Z., Wójcik Ł., Lis K. Determination of critical damage function values of CW008A copper and S355 steel in tensile and torsion tests, *Advances in Science and Technology Research Journal* 2023; 17(2): 173–180, <https://doi.org/10.12913/22998624/161053>
 28. Kubit A., Macek W., Zielecki W., Szawara P., Kłonica M. Fracture surface topography parameters for S235JR steel adhesive joints after fatigue shear testing, *Advances in Science and Technology Research Journal* 2023; 17(5): 130–139, <https://doi.org/10.12913/22998624/171490>
 29. Achtelek A., Kurek M., Kurek A., Kluger K., Pawliczek R., Łagoda T. Non-standard fatigue stands for material testing under bending and torsion loading. *AIP Conference Proceedings* 2029. *Mechatronic Systems and Materials* 2018. 020001-1-020001-14.
 30. Strzelecki P., Mazurkiewicz A., Musiał J., Tomaszewski T., Słomion M. Fatigue life for different stress concentration factors for stainless steel 1.4301,

- Materials 2019; 12: 3677.
31. Strzelecki P., Wachowski M. Effect of the stress concentration factor on the final fracture zone of aluminium AW 6063 T6 for rotating bending specimens. *Materials Today Communications* 2022; 31: 103766; <https://doi.org/10.1016/j.mtcomm.2022.103766>
 32. Leach R. (ed.), *Characterisation of Areal Surface Texture*. Springer-Verlag, Berlin-Heidelberg; 2013.
 33. https://www.keyence.eu/ss/products/microscope/roughness/surface/tab02_b.jsp
 34. Brown C.A., Charles P.D., Johnsen W.A., Chesters S. Fractal analysis of topographic data by the patchwork method. *Wear*, 1993; 161(1–2): 61–67, [https://doi.org/10.1016/0043-1648\(93\)90453-S](https://doi.org/10.1016/0043-1648(93)90453-S)
 35. Berkman F., Lemesle J., Guibert R., Wiczciorowski M., Brown C., Bigerelle M. Two 3D Fractal-Based Approaches for Topographical Characterization: Richardson Patchwork versus Sdr, *Materials*, 2024; 17: 2386. <https://doi.org/10.3390/ma17102386>
 36. Brown C.A., Siegmann S. Fundamental scales of adhesion and area–scale fractal analysis, *International Journal of Machine Tools & Manufacture* 2001; 41: 1927–1933, [https://doi.org/10.1016/S0890-6955\(01\)00057-8](https://doi.org/10.1016/S0890-6955(01)00057-8)
 37. Žak K., Grzesik W. Metrological aspects of surface topographies produced by different machining operations regarding their potential functionality. *Metrology and Measurement Systems* 2017; 24(2): <https://doi.org/10.1515/mms-2017-0027>